

The influence of fibril composition and dimension on the performance of paper gated oxide transistors

L Pereira¹, D Gaspar¹, D Guerin², A Delattre², E Fortunato¹ and R Martins¹

¹ CENIMAT/I3N, Departamento de Ciência dos Materiais, Faculdade de Ciências e Tecnologia, FCT, Universidade Nova de Lisboa, and CEMOP-UNINOVA, 2829-516 Caparica, Portugal

² CTP, Centre Technique du Papier, CS90251, Domaine Universitaire, Grenoble, France

E-mail: lmnp@fct.unl.pt and rm@uninova.pt

Received 4 August 2013, revised 3 October 2013

Published 12 February 2014

Abstract

Paper electronics is a topic of great interest due the possibility of having low-cost, disposable and recyclable electronic devices. The final goal is to make paper itself an active part of such devices. In this work we present new approaches in the selection of tailored paper, aiming to use it simultaneously as substrate and dielectric in oxide based paper field effect transistors (FETs). From the work performed, it was observed that the gate leakage current in paper FETs can be reduced using a dense microfiber/nanofiber cellulose paper as the dielectric. Also, the stability of these devices against changes in relative humidity is improved. On other hand, if the pH of the microfiber/nanofiber cellulose pulp is modified by the addition of HCl, the saturation mobility of the devices increases up to $16 \text{ cm}^2 \text{ V}^{-1} \text{ s}^{-1}$, with an $I_{\text{ON}}/I_{\text{OFF}}$ ratio close to 10^5 .

Keywords: paper electronics, paper transistors, nanodielectrics

 Online supplementary data available from stacks.iop.org/Nano/25/094007/mmedia

(Some figures may appear in colour only in the online journal)

1. Introduction

Sustainability has become an all-important feature for the development of new electronic products. Disposable consumer electronics is a really hot topic because new markets are constantly being created, resulting in an enormous stress on demand for raw materials but also problems of electronic waste management. Therefore eco-friendly materials and products are of extreme interest, both for these new products and markets and to replace or complement the existing ones. Paper electronics is considered a promising technology, able to overcome some of the problems mentioned above [1]. Despite being still far from achieving mass production, remarkable advances in materials science and simplified manufacturing processes are establishing the foundations for a whole new generation of cheap, bendable, disposable, biodegradable and recyclable electronics.

The strong interest among the scientific and industrial community in the production of electronic or electrochemical devices on paper substrates is mainly driven by its low cost ($\approx 10^{-3}$ cent m^{-2} , more than an order of magnitude cheaper than polyethylene terephthalate—PET), light weight, flexibility and ability to be 100% recyclable. Moreover, cellulose is the Earth's major biopolymer, the yearly production of paper is about 100 million tons and its production technology is state of the art, where the process speed (roll-to-roll—R2R—manufacturing) can exceed 100 km h^{-1} . Several attempts have been made to exploit the potential of paper as a substrate for low-cost and flexible electronics [2, 3]. Most common applications of paper are as dielectrics for capacitors [4, 5] and supercapacitors [5], permeable membranes in liquid electrolyte batteries [6, 7], microfluid channels [8, 9] and simply physical supports for energy storage devices [10, 11], organic thin film transistors (OTFTs) [11–13], printed

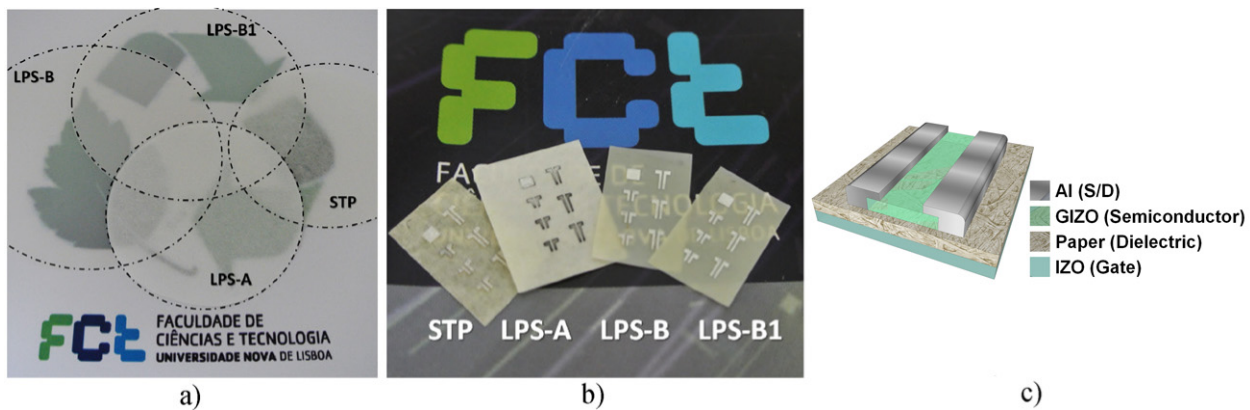


Figure 1. Photographs of (a) paper samples used in this work and (b) FETs produced on them; (c) schematic representation of the FET cross section.

sensors and RFID tags [14], printed batteries [15], inorganic powder electroluminescence devices [16], foldable printed circuit boards [17], oxide field effect transistors (FETs) [18] and flexible low voltage electric double-layer TFTs [19].

Our group has developed pioneer work giving to paper new functionalities and showing that paper can be used not only as a substrate but also as the dielectric for devices based on semiconductor oxides, such as FETs [20], memory transistors [21] and CMOS devices [22, 23]. Oxides are an interesting option for producing transistors on paper with good electrical performance because high quality semiconductor and conductor layers can be prepared at low temperatures [20, 24]. Indeed giving new functionalities to paper became a hot topic recently. Most of the efforts have been devoted to turning cellulose substrates electrically conductive either by just depositing transparent conductive oxides on it [25] or through real functionalization of cellulose nanofibers with either conductive polymers [26], carbon nanotubes (CNTs) [27, 28] or graphene [29]. Apart from that, the functionalization of microfibrils has also been proposed to produce p–n based cellulose rectifiers [30]. On the other hand not much can be found in the literature about the optimization of cellulose based substrates to be used as dielectric in FETs. In this work we demonstrate that paper substrates produced from microfibril–nanofibril cellulose has a strong influence on the performance of oxide based FETs. The effect of the fiber’s type, structure and dimension is studied as regards the use of the paper as a dielectric in such devices.

2. Experiments

2.1. Paper samples

In this work we have used four different kinds of paper substrates: standard tracing paper (STP) and lab paper samples (LPS) A, B and B1 with thickness of 75, 63, 51 and 52 μm , respectively (figure 1(a)). LPS-A is a 57 g m^{-2} paper made from only bleached softwood Kraft pulp. LPS-B is 41 g m^{-2} paper made from microfibrillated/nanofibrillated cellulose (M-NFC). The M-NFCs were produced from a mixed hardwood pulp subjected to a mechanical/enzymatic pre-treatment

followed by a homogenizing step. The B1 sample is the same as B, but in it HCl was added during the preparation of the diluted suspension of M-NFC before paper formation, in order to decrease the pH to 5.5. The three laboratory paper samples were manufactured by Centre Technique du Papier (CTP) using a lab handsheet former. For more details about the preparation and characteristics of paper please see the supplementary information (available at stacks.iop.org/Nano/25/094007/mmedia).

2.2. Paper characterization

The paper surface morphology was evaluated by scanning electron microscopy (SEM, with a Zeiss Auriga Crossbeam microscope). The structure of the paper was studied by means of x-ray diffraction (XRD; PANalytical, model X’Pert Pro) in Bragg–Brentano geometry with Cu $K\alpha$ line radiation ($\lambda = 1.5406 \text{ \AA}$). The XRD patterns were collected with a scanning step of 0.0334° over the angular 2θ range 10° – 70° .

Fourier transform infra-red (FTIR) spectroscopy was used to infer water content variations in the paper. The spectra were acquired between 4000 and 650 cm^{-1} with a 4 cm^{-1} step using an attenuated total reflectance (ATR) sampling accessory (Smart iTR) equipped with a single-bounce diamond crystal on a Thermo Nicolet 6700 Spectrometer.

The capacitance variation with frequency (C – f) was determined by impedance spectroscopy using a Gamry Instruments Reference 600 Potentiostat in a frequency range of 10 mHz – 1 MHz with an ac excitation voltage of 500 mV . For the metal–insulator–metal structures used for these measurements (4 cm^2 area), aluminum (Al) was evaporated through a metallic shadow mask on both sides of the paper.

Both FTIR-ATR and capacitance measurements were also performed under vacuum. The vacuum level was of the order of 0.2 Pa after 5 min, reaching 0.04 Pa after 1 h.

2.3. FETs production and characterization

The devices were produced on both sides of the paper with a staggered-bottom gate FET structure as can be seen in figures 1(b) and (c), without any previous surface treatment.

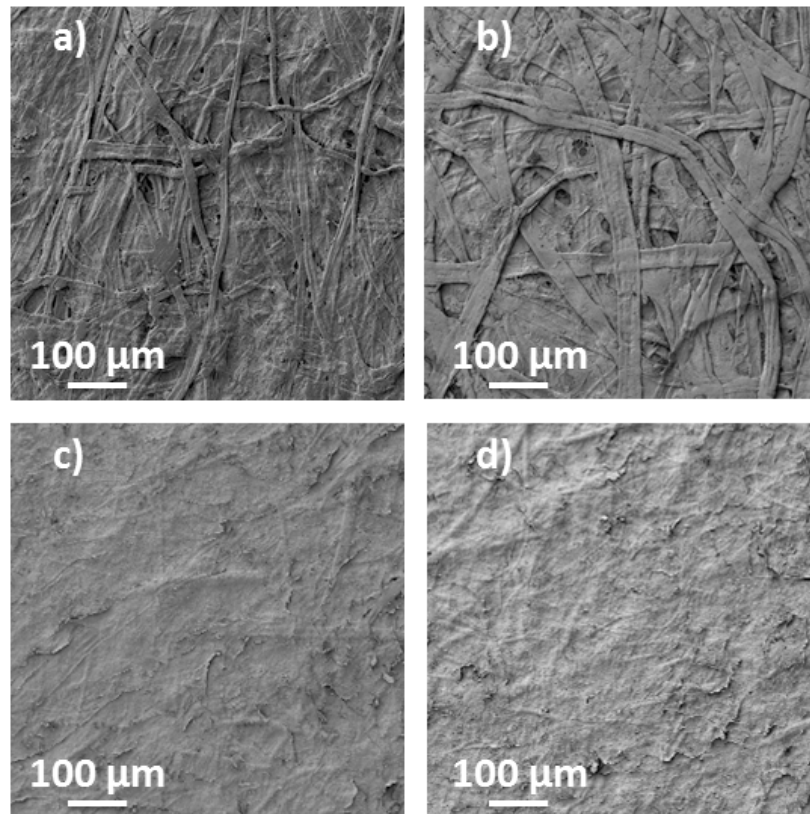


Figure 2. SEM micrographs of the four paper samples: (a) standard tracing paper (STP), (b) laboratory paper sample A (LPS-A), (c) M-NFC laboratory paper sample B (LPS-B) and (d) M-NFC laboratory paper sample B1 (LPS-B1).

On one side a 40 nm thick GIZO ($\text{Ga}_2\text{O}_3\text{-In}_2\text{O}_3\text{-ZnO}$; 1:2:2% mol) film was deposited by RF magnetron sputtering through a shadow mask in order to create the channel region [31]. Then, Al source/drain (S/D) electrodes (200 nm thick) were also deposited through a shadow mask by e-beam evaporation. Finally, a 200 nm thick IZO ($\text{In}_2\text{O}_3\text{-ZnO}$; 89.3:10.7 wt%) film was deposited on the other side of the paper substrate to be used as the gate (G) electrode. The sheet resistance of the IZO film deposited on paper is around $50 \Omega \text{ cm}$. The paper FETs were then annealed in air for 30 min at 150°C .

The transfer characteristics of the paper FETs with a channel width (W) of $1390 \mu\text{m}$ and length (L) of $210 \mu\text{m}$ ($W/L = 6.6$) were measured both at atmospheric pressure (23°C , and relative humidity of 40%), and under vacuum, using a microprobe station (Janis Research Company) connected to a semiconductor parameter analyzer (Agilent 4155C). In order to evaluate the stability of the FETs under bending, the transfer characteristics were also measured with the paper substrates bent (bending radius of 45, 25, 15 and 5 mm) along an axis running through the channel, parallel to the source and drain electrodes.

3. Results and discussion

3.1. Paper substrates

The SEM micrographs presented in figure 2 show the differences in morphology of the paper samples used. The

smoothest and more homogeneous surfaces are obtained on the M-NFC papers (LPS-B and B1) as a result of the small fibril dimension which leads to highly compact paper structures (density 1250 and 1290 kg m^{-3} respectively), even if not calendered (see the supplementary information available at stacks.iop.org/Nano/25/094007/mmedia). The images also show that the fibril size is not uniform, with some elements having length greater than $100 \mu\text{m}$, embedded in a matrix constituted from smaller ones (see the supplementary information (available at stacks.iop.org/Nano/25/094007/mmedia) figure 4 for more detailed analysis on paper roughness).

On the other hand, large fibers with dimensions sometimes exceeding $500 \mu\text{m}$ in length and $50 \mu\text{m}$ in width are identified in the LPS-A sample. These are wider than those of STP, which is related to the fiber source (mixed hardwood/softwood for STP and softwood only for LPS-A).

The crystallinity index (I_c) of the paper samples was determined from XRD data (figure 3) using the empirical method proposed by Segal *et al* [32]:

$$I_c = \frac{I_{(002)} - I_{(\text{am})}}{I_{(002)}} \times 100 \quad (1)$$

where $I_{(002)}$ is the maximum intensity of the diffraction of the (002) lattice peak and $I_{(\text{am})}$ is the intensity of the diffraction of the amorphous phase, taken at the minimum on a 2θ angle range between 18° and 20° . It should be noted that the

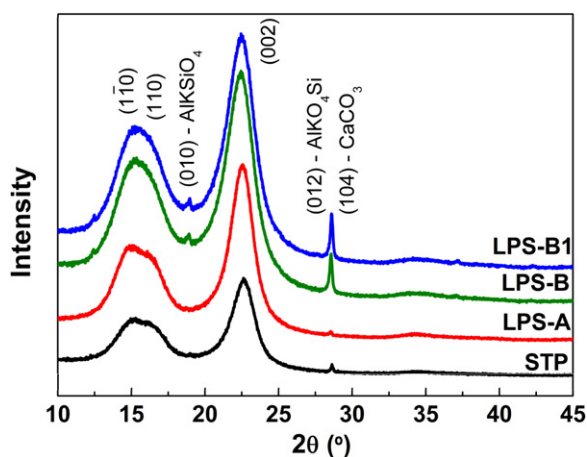


Figure 3. XRD diffractograms of reference and laboratory prepared paper samples. Typical (110), (110) and (002) diffraction peaks of cellulose I (native cellulose [33]) are identified.

crystallinity index estimated through this method is interesting only for comparison between samples, because accurate values are difficult to determine as they vary significantly, depending on the technique and calculation method used [33]. The LPS-B and B1 paper (M-NFC) present the lowest I_c (around 71%), which is directly related to the cellulose fiber source and the pulping method used. The M-NFC is produced from a mixed hardwood pulp obtained through a mechanical refining and enzymatic treatment to gradually reduce the size of the fibers and open the cell wall structure. This increases the surface roughness and causes disorder in superficial cellulose chains [34, 35]. The small dimension of the fibrils results in high surface area, meaning that the ratio between disordered surface chains and internal ones is higher than for large fibers, which contributes to the reduction of the crystalline fraction. The decrease of the crystallinity along with the homogenizing steps has already been shown by Larsson *et al* using carbon 13 NMR [36].

STP and LPS-A paper samples present similar crystalline fractions (around 87% for both). Not much is known about the process of production of STP but it is supposed to be a mix of some bleached softwood and hardwood Kraft pulp, as usual in the paper industry. Since the hardwood pulp has higher content of hemicelluloses (usually amorphous regions) than softwood ones, this also contributes to the lower crystallinity index of M-NFC papers.

The LPS-B and B1 diffractograms in figure 3 show an intense peak around 28° that we associate with the presence of calcite (CaCO_3) and kalsilite (KAlSiO_4) in the paper. These peaks are also detectable for STP and LPS-A paper samples, although they are not as intense as for M-NFC papers. Another peak for the 2θ angle of 18.9° can also be ascribed to kalsilite. These compounds are external contamination of the LPS papers resulting either from pigments that are commonly used in papermaking (calcium carbonate and clay) or from the water mineral content. It must be noted that M-NFC exhibits higher surface area (about ten to hundreds of $\text{m}^2 \text{g}^{-1}$) than conventional fibers ($1\text{--}3 \text{m}^2 \text{g}^{-1}$) and that the zeta potential (ZP) of the M-NFC is significantly lower (-44mV for a

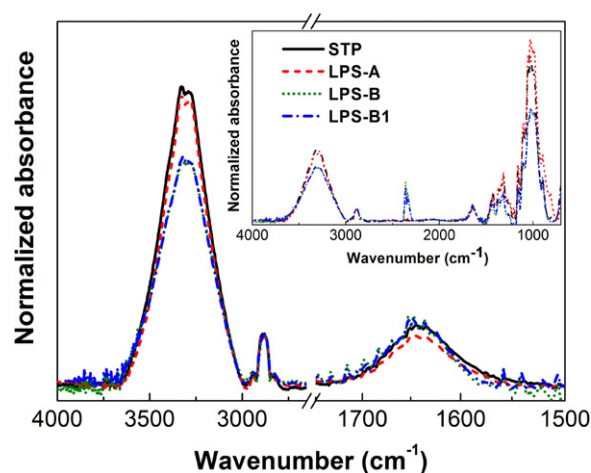


Figure 4. ATR-FTIR spectra of the different paper samples normalized to the intensity of the band at 2900cm^{-1} . The figure shows magnification of the bands at $3600\text{--}3000 \text{cm}^{-1}$ and at 1635cm^{-1} while the entire spectra are shown in the inset.

diluted suspension at $1200 \mu\text{S cm}^{-1}$) than that of conventional pulp (normally around -15mV). As wood pulp is known to adsorb metal cations [37], this phenomenon is expected to be magnified when producing M-NFC.

ATR-FTIR spectra are shown in figure 4, where the characteristic absorption bands for cellulose are found, such as the hydrogen-bonded OH stretching at $3600\text{--}3000 \text{cm}^{-1}$, the C-H stretching at 2900cm^{-1} and other specific bands assigned to cellulose, hemicelluloses and lignin in the $1800\text{--}600 \text{cm}^{-1}$ fingerprint area [38–41]. The spectra were normalized to the intensity of the band at 2900cm^{-1} which is quite insensitive to variations in the composition, crystallinity and water content of the cellulose [42].

The FTIR spectra of paper are deeply influenced by the adsorbed water. The band at approximately 700cm^{-1} (see figure 4 inset) has been assigned to the out-of-plane vibrations of OH groups [43] or to rotational vibrations of the whole H_2O molecule [44], while the one at 1635cm^{-1} is associated with the OH bending of adsorbed water [45]. Figure 4 shows that there is no clear difference in the water content of the samples that can be evaluated via the evolution of the band at 1635cm^{-1} [39]. Nevertheless the broad band between 3600 and 3000cm^{-1} can be used to infer how water sorbs at the fiber surface, as it can result from water strongly bound by hydrogen bonds to the OH groups and more loosely bound water indirectly bonded to the OH groups via another water molecule. This band is more intense for STP and LPS-A than for M-NFC papers which means that the water is preferentially sorbed (either strongly or weakly) by hydroxyl groups at the fiber surface, in the form of freezing bound water [46]. On the other hand, it is also known that hardwood pulp used as a source of M-NFCs contains a high amount of amorphous hemicelluloses (even after Kraft pulping) and so of carboxylated groups that can bond to water as well. Finally one must also consider the formation of calcite and kalsilite since these two compounds are highly hygroscopic [47] and affect the water content in the M-NFC paper samples.

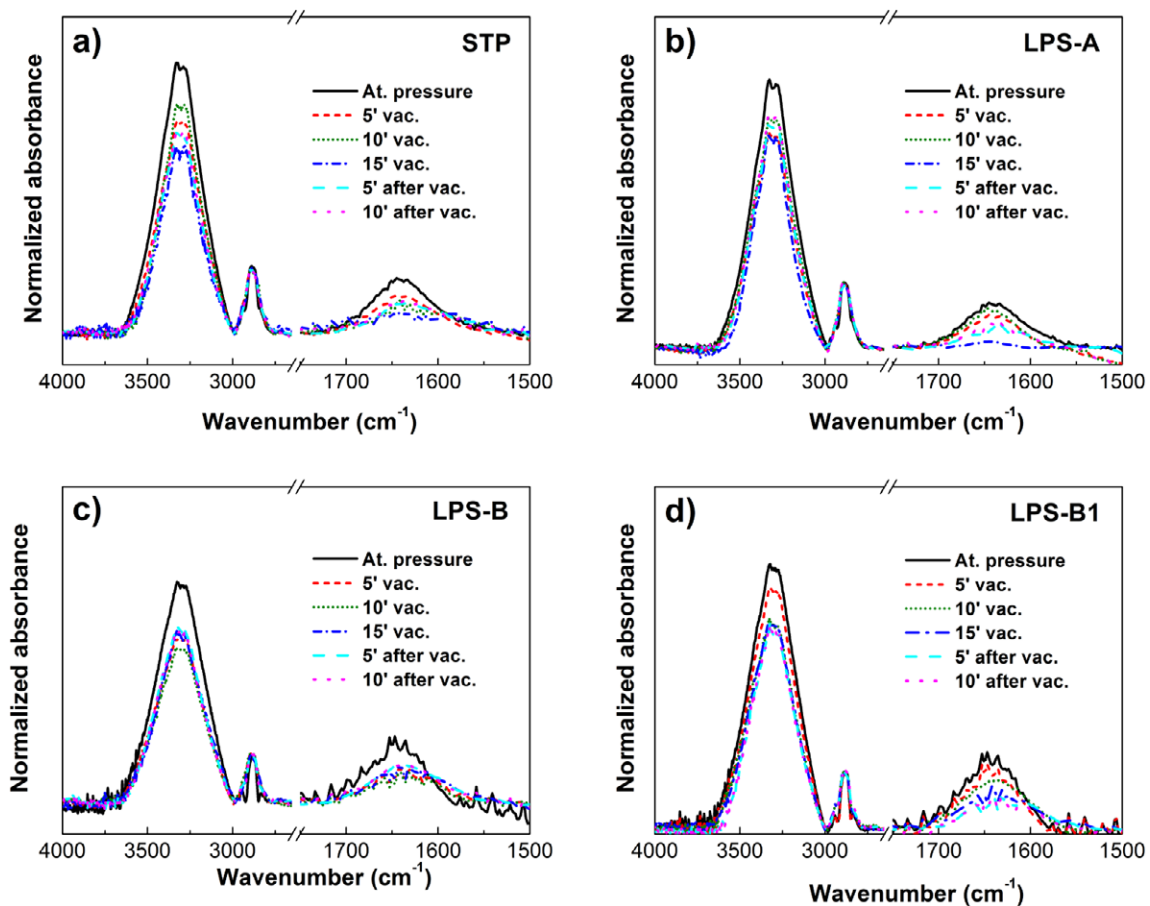


Figure 5. Detailed ATR-FTIR spectra of the bands at $3600\text{--}3000\text{ cm}^{-1}$ and at 1635 cm^{-1} for (a) STP, (b) LPS-A, (c) LPS-B and (d) LPS-B1. The water content variation under vacuum and after recovery was analyzed via the changes in the intensity of these bands.

In order to check the sensitivity of paper samples to abrupt variations in the relative humidity, they were left in vacuum for various time intervals and the FTIR spectra were taken immediately after removing them from the vacuum chamber (figure 5). The reduction of the intensity of the broad band between 4000 and 3000 cm^{-1} and that at 1635 cm^{-1} after some minutes in vacuum for all samples means that the adsorbed water content decreases over time. In this analysis we must take into account the error induced by the time frame (of about a minute) that separates the moment when the samples are removed from the vacuum chamber and the measurement. During this period the samples may partially recover their water content, leading to wrong conclusions. Nevertheless, it is clear that the relative variation of the band at 1635 cm^{-1} in M-NFC paper (LPS-B and B1) is not as large as for STP and LPS-A. The spectra taken when the samples are left in environmental relative humidity conditions show that the water content recovery is faster for STP and LPS-A samples than for LPS-B and B1 ones. This is attributed to the more compact structure of the M-NFC papers, which affects the capacity of water for diffusing into the porous network, and the higher density of OH bonds between the fibrils in M-NFC compared to the fiber scale, which slows down the sorption/desorption rate.

The capacitance of the paper substrates as a function of the frequency ($C\text{--}f$) is shown in figure 6. Different polarization

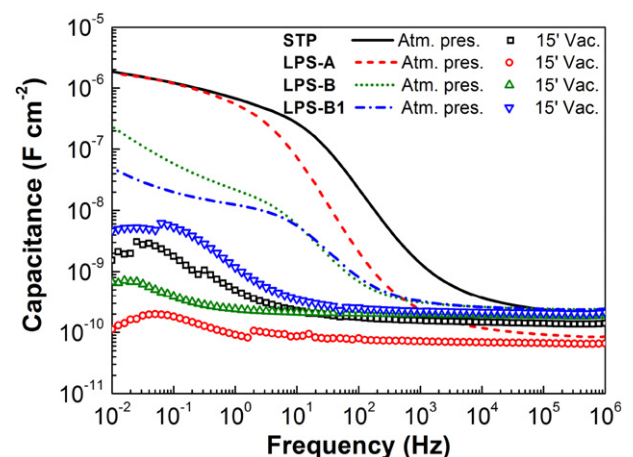


Figure 6. Capacitance variation with frequency ($C\text{--}f$) of the set of paper samples used. Solid and dashed lines represent the capacitance measured at atmospheric pressure while the open symbols represent the capacitance measured under vacuum after pumping for 15 min.

mechanisms are expected at different frequencies, namely dipolar (high frequencies), ionic (intermediate frequencies), and electrode interface-related relaxations (low frequencies). The strong increase in the capacitance at low frequencies is related to the presence of electrode polarization [48]. This

Table 1. Comparison of the electrical properties of GIZO based FETs with different paper samples as gate dielectrics.

	STP	LPS-A	LPS-B	LPS-B1
μ_{sat} ($\text{cm}^2 \text{V}^{-1} \text{s}^{-1}$)	2.3	0.14	0.94	16
V_{ON} (V)	-2.5	-5.5	-4.7	-4.8
$I_{\text{ON}}/I_{\text{OFF}}$	2.5×10^4	1.7×10^4	2.2×10^4	7.5×10^4
S (V/dec)	0.89	2.1	1.6	1.3
Capacitance ($\mu\text{F cm}^{-2}$)	1.7	1.8	0.24	0.05
Resistivity (Ωcm)	4.9×10^7	4.3×10^8	1.4×10^9	1.3×10^9
Thickness (μm)	75	63	51	52
Fiber average width/length (μm)	>500/~10	>1000/~20	>10/<0.1	>10/<0.1
RMS roughness (μm)	6.4	5.8	2.6	2.6

happens because of the interaction of the charged electrode surface with free charges in the paper, similar to what happens in electric double-layer (EDL) capacitors [49]. These EDLs are formed in a narrow region at the electrode surface (<10 nm, depending on electrolyte properties), resulting in a large capacitance that has been explored in decreasing the operational voltage of organic electrolyte gated transistors (EGT) [48, 50, 51] and also oxide based ones [52, 53]. This means that high capacitance can be obtained on paper at low frequencies regardless of its thickness.

The capacitance data presented in figure 6 indicate that paper behaves as an electrolyte when used as a dielectric in FETs and that the charge accumulation in the channel region in the steady state will occur through the formation of EDLs. In our previous work we had already predicted that the effective capacitance of paper could not be calculated by just using its high frequency dielectric constant since this would result in abnormally high saturation mobility (μ_{SAT}) in oxide based FETs, depending instead of the charge retained on the fibers surface that would be, theoretically, related to the paper's internal structure and morphology [20, 21, 54–56]. It is believed that the EDL formation (and capacitance increase at low frequencies) will depend on the free protons or ions existing in the paper near the electrode interface and as well as on their mobility, and both will depend on the sorbed water [48]. FTIR analysis has shown that water is sorbed in the paper which means that there is a source of some small ions such as protons (H^+) and hydroxyls (OH^-), resulting from water dissociation at the fiber surface, that are responsible for the build-up of the capacitance at low frequencies. This is corroborated by the strong decrease in the capacitance of the paper samples when it is measured in vacuum, due to the moisture loss. This confirms that water sorption is responsible for the formation of the EDL in paper, providing both negative and positive ions, making it suitable for used as a dielectric, on both n-type and p-type FETs [22, 23].

The capacitance values at 0.01 Hz for STP and LPS-A are 1.8 and 1.7 $\mu\text{F cm}^{-2}$, respectively, well above those of LPS-B and B1 (0.24 and 0.05 $\mu\text{F cm}^{-2}$, respectively). Ionized water is more strongly bound on M-NFCs, reducing the ionic mobility, and thus affecting the formation of the EDL at the paper surface. The capacitance for M-NFC papers follows an increasing tendency at 0.01 mHz, that suggests the existence

of another relaxation related to the contribution of strongly bound water.

FTIR characterization provides evidence that STP and LPS-A samples are more sensitive to abrupt variations in the relative humidity than the other paper samples. This is confirmed by the capacitance variation measured after 15 min in a vacuum, which is reduced by 3–4 orders of magnitude for STP and LPS-A samples. The less compact structure, together with a rough and less homogeneous surface, and/or weakly bound water at the fiber surface explains why the reduction is more accentuated here than for M-NFC papers. Indeed FTIR data show a more intense broad absorption band at 3600–3000 cm^{-1} for STP and LPS-A samples which suggests a high amount of weakly bound water in these papers. For instance, thermogravimetric analysis (see the supplementary information available at stacks.iop.org/Nano/25/094007/mmedia) shows an accentuated weight loss for the STP sample due to water desorption, that begins immediately after starting to heat the sample, thus confirming the presence of weakly bound water.

3.2. Paper FET electrical characteristics

The paper FET geometry is shown in figure 7, where it is possible to compare the device dimension with the fiber size and surface morphology, while the transfer characteristics ($I_{\text{DS}}-V_{\text{GS}}$) in the saturation regime ($V_{\text{DS}} = 15 \text{ V}$) of devices gated with paper are shown in figure 8(a) and the extracted electrical parameters are listed in table 1. The gate capacitance used for the calculation of the saturation mobility (μ_{SAT}) was taken from the $C-f$ measurements at 0.01 Hz, in order to take into account the EDL formation. Indeed the calculation of the mobility in devices gated with EDLs will depend on the frequency chosen to measure the capacitance. For instance, in the work of Lim *et al* [24] the capacitance at 1 MHz was used, not taking into account the possible formation of an EDL at the paper surface, which is likely to result in an overestimation of the mobility. Therefore, the lower the frequency used to determine the capacitance, the more accurate the value of the mobility calculated, as it gets closer to the steady state regime value, where the transfer characteristics are obtained.

The highest μ_{SAT} is obtained for M-NFC LPS-B1 paper (16 $\text{cm}^2 \text{V}^{-1} \text{s}^{-1}$). Despite not having the highest capacitance, this kind of paper is highly compact, has small dimension

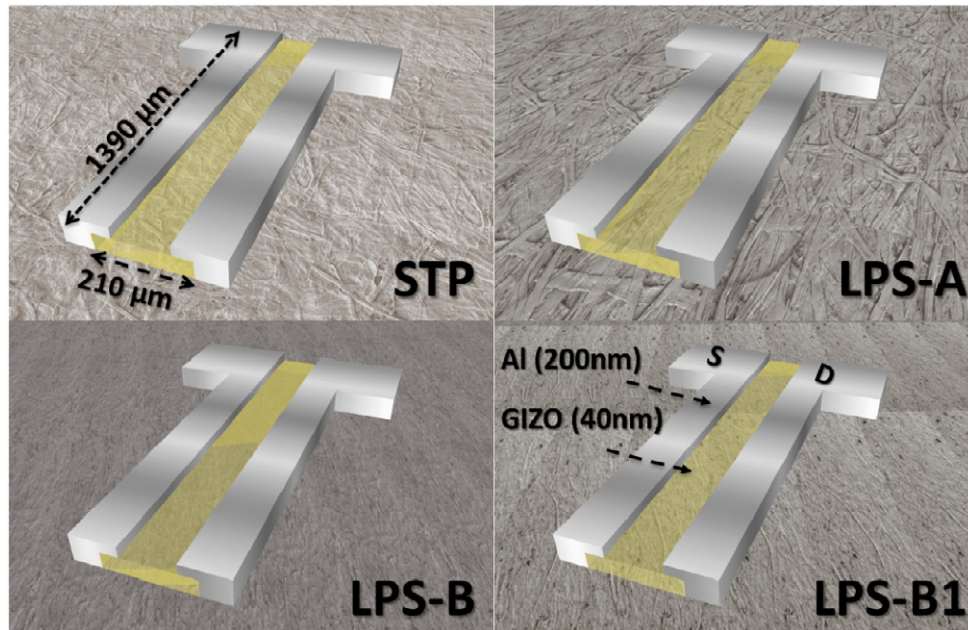


Figure 7. Scale 3D representation of the FET geometry on the paper surface showing how the transistor dimension compares with the fiber size and morphology. The thicknesses of GIZO and Al are not to scale, in order to show the transistor structure better.

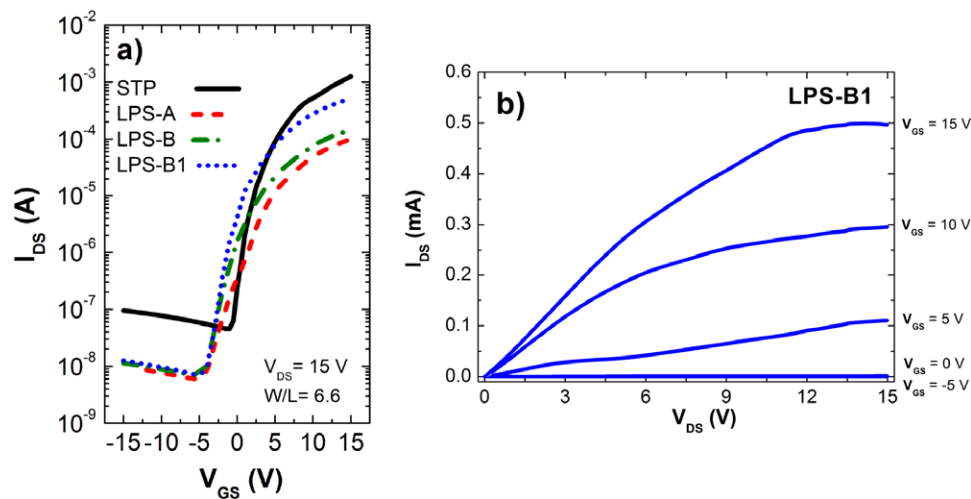


Figure 8. (a) I_{DS} – V_{GS} transfer characteristics of the paper gated GIZO FETs at $V_{DS} = 15$ V (saturation regime). (b) Output characteristics of the GIZO FET on LPS-B1 paper.

fibrils, and also has a relatively smooth surface for a paper sheet (RMS roughness of about $2.6 \mu\text{m}$; see figure 4 in the supplementary information available at stacks.iop.org/Nano/25/094007/mmedia) which results in FETs with very interesting electrical characteristics. The difference in maximum value of the ON currents (I_{ON}) of LPS-B and B1 paper based FETs is explained by H^+ sorption at the GIZO surface. During the LPS-B1 paper formation, HCl was added to the fibril suspension, hence decreasing its pH to 5.5, and thus creating an extra density of protons at the fibril surface. This resulted in a paper with a surface pH of 5.8, compared to 7.0 for the LPS-B sample. It was shown by Juan *et al* that H^+ can bond to a ZnO surface under gate bias through chemisorption or physisorption reducing its sheet resistance [53]. This explains

why the current and the mobility for the LPS-B1 FET are higher than for that on LPS-B, even if the capacitance measured for the Al–paper–Al capacitor is lower.

We noticed that the main limitation of these paper FETs is related to the I_{ON}/I_{OFF} ratio whose maximum is 7.5×10^4 for transistors on LPS-B1 paper. I_{OFF} is clearly governed by the gate leakage current (I_{GS}) which is reduced by one order of magnitude on M-NFC papers, as compared with the STP one (see figure 10). The values obtained are in line with the resistivity of the paper as determined by impedance spectroscopy (see table 1 and the supplementary information available at stacks.iop.org/Nano/25/094007/mmedia). The highest resistivity was obtained in M-NFC papers due to the low mobility of H^+ and OH^- , as these ions make an important contribution to the electrical conductivity.

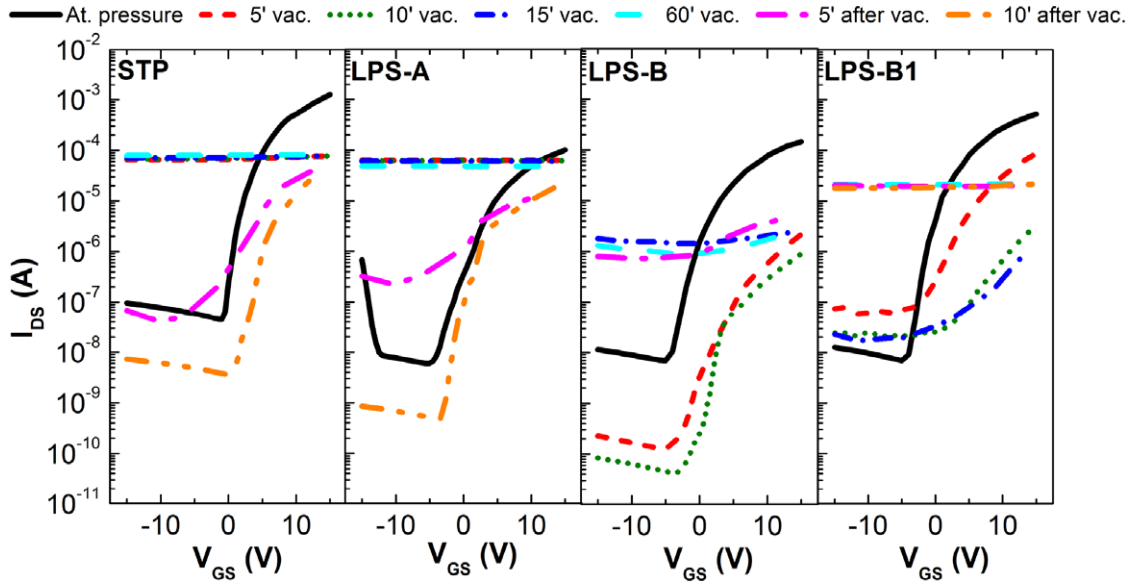


Figure 9. I_{DS} - V_{GS} transfer characteristics of the paper gated GIZO FETs at $V_{DS} = 15$ V (saturation regime) obtained under vacuum and after recovery at atmospheric pressure. The initial transfer characteristics are also presented for comparison.

We must not ignore that the mobility on STP and LPS-A paper based FETs can be underestimated since we have considered an effective width/Length (W/L) ratio of 6.6, which might not really be the case for rough papers, as the GIZO layer is only 40 nm and cannot make a good step coverage on the rough surface of STP and LPS-A papers. This means that the path between the source and the drain is made on top of just some randomly oriented fibers [54], resulting in an L higher than 210 μm , while the effective W should be less than 1390 μm . This effect will be attenuated as the surface roughness of the paper decreases and the effective GIZO area coverage approaches that of the geometrical W and L dimensions.

Figure 8(b) shows the typical output characteristics (V_{DS} - I_{DS}) for GIZO FETs on LPS-B1 paper. They exhibit current saturation behavior, meaning that the semiconductor is depleted under the drain electrode (pinch off). A saturation current of 0.5 mA is obtained at $V_{GS} = 15$ V. Current crowding in the low drain voltage region is visible, indicating that the device performance is partially affected by the source and drain contact resistance which is related to non-ideal fiber step coverage by a 40 nm thick semiconductor layer, as mentioned above [54]. Similar behavior was observed for all other papers FETs.

The transfer characteristics of the FETs measured at atmospheric pressure and under vacuum conditions are presented in figure 9. The vacuum level was of the order of 0.2 Pa after 5 min, reaching 0.04 Pa after 1 h.

The data clearly confirm that STP and LPS-A paper based FETs are more sensitive to relative humidity changes than the M-NFC ones. As soon as the pressure drops inside the chamber, the water desorption occurs and the devices show no current modulation. The exact moment when this occurs was not determined, since the first measurement was taken after 5 min. This is not the case for devices gated with

LPS-B paper dielectric which still show current modulation after being under vacuum conditions for 10 min, while the ones based on LPS-B1 paper are still working after 15 min under vacuum conditions. We also notice that, overall, when the vacuum chamber is vented, the FETs on STP and LPS-A papers recover the transistor characteristics faster than those on M-NFC paper. Indeed the FETs on LPS-B1 paper do not show any modulation even after recovering for 10 min under atmospheric pressure conditions.

The values of I_{GS} taken at atmospheric pressure and under vacuum conditions for devices on STP and LPS-B paper are shown in figure 10. There it is possible to see that the gate current decreases at a slower rate for M-NFC paper FETs than for the others. When the devices are brought again to atmospheric pressure, it takes longer to recover the original value. As explained above, I_{GS} is highly dependent on the water content in the paper and these results confirm that the water desorption/sorption process is slower for M-NFC paper as compared with STP, leading to less sensitivity to abrupt changes in the relative humidity, as suggested by ATR-FTIR results.

The electrical characteristics of the paper based FETs were also evaluated under tensile bending strain. The strain (ε) for a flexible substrate more compliant than the thin film deposited on it and that it is bent to an inner radius (r) was determined following [57]:

$$\varepsilon = \frac{(d_f + d_s)}{2r} \frac{(1 + 2\eta + \chi\eta^2)}{(1 + \eta)(1 + \chi\eta)} \quad (2)$$

where d_f and d_s are the film and substrate thicknesses, respectively, η is the d_f/d_s ratio and χ is the Young moduli (E_f/E_s) ratio. Taking into account the thickness of the GIZO films used and that η is around 10^3 , which compensates for the difference in Young modulus of paper and oxide thin films,

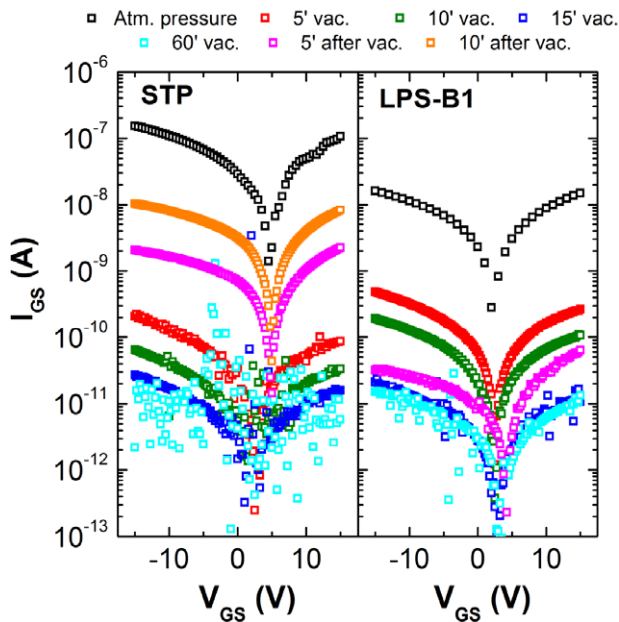


Figure 10. Gate leakage current (I_{GS}) evolution when the measurements are made on the devices under vacuum and after recovery at atmospheric pressure for 5 and 10 min. The initial currents I_{GS} are also presented for comparison.

equation (2) is simplified to

$$\varepsilon \approx \frac{(d_f + d_s)}{2r} \quad (3)$$

which means that the midsurface of the paper substrate is the neutral surface. Figure 11 shows the relative variation of μ_{SAT} (μ/μ_0), the I_{ON}/I_{OFF} ratio (I/I_0) and S (S/S_0) when the measurements are made on the STP and LPS-B1 devices under tensile bending strain. It is remarkable that the devices on both papers still present excellent electrical performance even at a bending radius of 5 mm. For instance, Someya et al obtained 3.5 mm as the maximum bending radius for pentacene TFTs

on polyimide substrates without an encapsulation stack [58]. Nevertheless the electrical characteristics of the FETs present some variation, namely μ_{SAT} and I_{ON}/I_{OFF} that are much more sensitive than S . It is interesting to note that the device produced on STP paper presents first an increase in μ_{SAT} as ε increases up to 0.25%, followed by a decrease of such parameters for $\varepsilon = 0.75\%$ (corresponding to a bending radius of 15 mm). On the other hand, μ_{SAT} and the I_{ON}/I_{OFF} ratio of the device on LPS-B1 paper start by decreasing under tensile strain. Another important point is that the device on STP paper recovers its initial characteristics when measurements are made again for a flat condition after bending (open symbols) while μ_{SAT} for the FET produced on LPS-B1 is reduced, as a result of the decrease in the source–drain current which also affects negatively the I_{ON}/I_{OFF} ratio. There is no evident explanation for this difference in behavior and one can only speculate that it is related to the different fiber sizes of the papers. The channel of the FET on STP is not continuous, being formed of top of the tangled large fibers that exist between the source and drain. Under bending conditions these large fibers are able to rearrange and accommodate the strain, without significantly damaging the oxide layer on top, while M-NFC paper is more brittle than the STP and the devices will suffer from some irreversible local damage that will reduce the ON current of the FETs.

Finally, a simple analysis of I_{DS} when applying a square wave gate voltage ($-20 \text{ V} < V_{GS} < 20 \text{ V}$) was done. Different frequencies were used in order to make inferences about the dynamic response of these devices. If one is simply considering the variation on the I_{ON}/I_{OFF} ratio, one can have a sense of magnitude of the switching frequency (where it is no longer possible to distinguish between states, that is, the point at which I_{ON}/I_{OFF} is 1). For devices produced on STP and LPS-A papers this occurs above 10 Hz while for FETs on M-NFC papers it occurs in the region between 1 and 10 Hz (see the supplementary information figure 5 available at stacks.iop.org/Nano/25/094007/mmedia). The limitation in the operation speed was expected since the device geometry

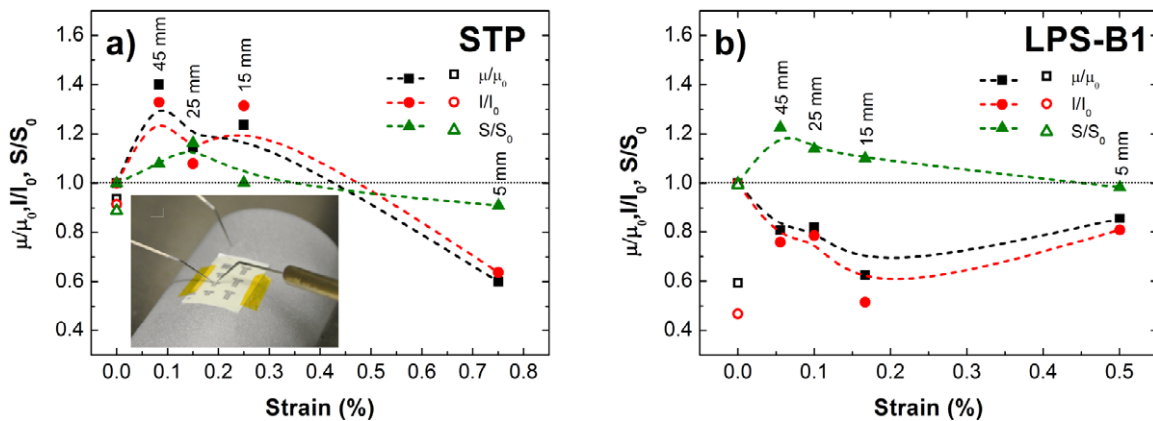


Figure 11. Normalized values of μ_{SAT} (μ/μ_0), the I_{ON}/I_{OFF} ratio (I/I_0) and S (S/S_0) for FETs on (a) STP and (b) LPS-B1 papers determined after measuring the transfer characteristics under tensile bending strain. The bending radius is presented next to the symbols. Open symbols represent the values calculated for a flat condition after bending. The inset shows a picture of the FETs on which the measurements were made under bending conditions.

was not optimized. The FET dimensions and the large source/drain to gate overlap result in large gate and parasitic capacitances that are not compatible with high operation speed. Improvements could be achieved through proper architecture design. However, the polarization response time of the paper will be the ultimate speed limiting factor. Ions must move to the interface to establish the EDL and the time taken by this process will depend on the resistance of the paper and its interfacial capacitance. This means that for paper sheets of some tenths of microns it will be hard to achieve devices operating above the kHz regime. Indeed 1–10 kHz is the maximum operation frequency for optimized devices gated with EDLs formed using ionic gels [59]. At present this limits the range of application to systems not requiring high switching speeds such as paper electrochromic displays (switching times in the range of 3–20 ms) and power controllers of energy sources to be used on paper (tags, smart labels and packaging, for instance).

4. Conclusions

It was successfully demonstrated that smooth and compact M-NFC paper can be used as the dielectric in oxide based FETs processed at low temperatures with excellent electrical performances and remarkable stability under bending. The device characteristics were compared with those produced on a wood fiber paper and a reference paper used in previous works [20, 21] and can compete with those for devices processed with other substrates such polymer or glass. The FETs produced on M-NFC paper exhibited a saturation mobility up to $16 \text{ cm}^2 \text{ V}^{-1} \text{ s}^{-1}$ and an $I_{\text{ON}}/I_{\text{OFF}}$ ratio close to 10^5 , being simultaneously less sensitive to abrupt changes in the relative humidity than conventional pulp papers. The small fibrils (width in the nanoscale range) and their surface properties (compact and smooth) strongly bind water to M-NFC paper, which is very important since it is an ion source, thus allowing for the formation of EDLs at the interface of paper with the GIZO. This shows that tailored low-cost and eco-friendly paper substrates can be used as functional material for flexible electronics in which they are not only the support but also a constituent of the devices themselves, whose performances can be properly tuned using M-NFC paper. Nevertheless we notice that the present switching times are high, limiting the field of applications; this means that further work is needed to reduce it.

Acknowledgments

This work was financed by the European Commission under projects INVISIBLE (FP7 ERC grant 228144), A3Ple (FP7, NMP-2010-SME-4 grant 262782), ORAMA (FP7, NMP3-LA-2010 grant 246334), and the Portuguese Science Foundation (FCT-MEC) through the Projects PEst-C/CTM/LA0025/2013–14, EXCL/CTM-NAN/0201/2012 and PTDC/CTM/103465/2008.

The authors would like to thank their colleagues Daniela Nunes, Sónia Pereira, Mafalda Costa and Ana Pimentel, for the SEM, XRD, confocal microscopy/3D profilometer and TG measurements, respectively.

References

- [1] Tobjörk D and Österbacka R 2011 Paper electronics *Adv. Mater.* **23** 1935
- [2] Kim D H, Kim Y S, Wu J, Liu Z, Song J, Kim H S, Huang Y Y, Hwang K C and Rogers J A 2009 Ultrathin silicon circuits with strain-isolation layers and mesh layouts for high-performance electronics on fabric, Vinyl, leather, and paper *Adv. Mater.* **21** 3703
- [3] Manekkathod A, Lu M Y, Wang C W and Chen L J 2010 Direct growth of aligned zinc oxide nanorods on paper substrates for low-cost flexible electronics *Adv. Mater.* **22** 4059
- [4] Tanaka Y, Hara R, Ishii N and Okura J 1999 Electric double layer capacitor having a separator made from a cellulose fiber *US Patent Specification* 5963419
- [5] Pushparaj V L, Shaijumon M M, Kumar A, Murugesan S, Ci L, Vajtai R, Linhardt R J, Nalamasu O and Ajayan P M 2007 Flexible energy storage devices based on nanocomposite paper *Proc. Natl Acad. Sci. USA* **104** 13574
- [6] Lee K B 2006 Two-step activation of paper batteries for high power generation: design and fabrication of biofluid- and water-activated paper batteries *J. Micromech. Microeng.* **16** 2312
- [7] Nystrom G, Razaq A, Strømme M, Nyholm L and Mhramyan A 2009 Ultrafast all-polymer paper-based batteries *Nano Lett.* **9** 3635
- [8] Carrilho E, Martinez A W and Whitesides G M 2009 Understanding wax printing: a simple micropatterning process for paper-based microfluidics *Anal. Chem.* **81** 7091–5
- [9] Veigas B, Jacob J M, Costa M N, Santos D S, Viveiros M, Inacio J, Martins R, Barquinha P, Fortunato E and Baptista P V 2012 Gold on paper–paper platform for Au-nanoprobe TB detection *Lab Chip* **12** 4802–488
- [10] Kucherovsky J J, Simmons G R, Miller J A and Mlnarik C F 2002 Method of making a thin film battery *Patent US Specification* 6379835
- [11] Kim Y H, Moon D G and Han J I 2004 Organic TFT array on a paper substrate *IEEE Electron Device Lett.* **25** 702–4
- [12] Huang J, Zhu H, Chen Y, Preston C, Rohrbach K, Cumings J and Hu L 2004 Highly transparent and flexible nanopaper transistors *ACS Nano* **7** 2106–13
- [13] Eder F, Klauk H, Halik M, Zschieschang U, Schmid G and Dehm C 2004 Organic electronics on paper *Appl. Phys. Lett.* **84** 2673–5
- [14] Yang L, Rida A, Vyas R and Tentzeris M M 2007 RFID tag and RF structures on a paper substrate using inkjet-printing technology *IEEE Trans. Microw. Theory Tech.* **55** 2894
- [15] Hilder M, Winther-Jensen B and Clark N B 2009 Paper-based, printed zinc–air battery *J. Power Sources* **194** 1135
- [16] Kim J Y, Park S H, Jeong T, Bae M J, Song S, Lee J, Han I T, Jung D and Yu S G 2010 Paper as a substrate for inorganic powder electroluminescence devices *IEEE Trans. Electron Devices* **57** 1470
- [17] Siegel A C, Phillips S T, Dickey M D, Lu N, Suo Z and Whitesides G M 2010 Foldable printed circuit boards on paper substrates *Adv. Funct. Mater.* **20** 28–35
- [18] Lim W, Douglas E A, Norton D P, Pearton S J, Ren F, Heo Y W, Son S Y and Yuh J H 2010 Low-voltage indium gallium zinc oxide thin film transistors on paper substrates *Appl. Phys. Lett.* **96** 053510
- [19] Lu A X, Dai M, Sun J, Jiang J and Wan Q 2011 Flexible low-voltage EDL TFTs self-assembled on paper substrates *IEEE Electron Device Lett.* **32** 518
- [20] Fortunato E, Correia N, Barquinha P, Pereira L, Goncalves G and Martins R 2008 High-performance flexible hybrid field-effect transistors based on cellulose paper *IEEE Electron Device Lett.* **29** 988

- [21] Martins R, Barquinha P, Pereira L, Correia N, Gonçalves G, Ferreira I and Fortunato E 2008 Write-erase and read paper memory transistor *Appl. Phys. Lett.* **93** 203501
- [22] Martins R, Nathan A, Barros R, Pereira L, Barquinha P, Correia N, Costa R, Ahnood A, Ferreira I and Fortunato E 2011 Complementary metal oxide semiconductor technology with and on paper *Adv. Mater.* **23** 4491
- [23] Martins R, Ahnood A, Correia N, Pereira L, Barros R, Barquinha P, Costa R, Ferreira I, Nathan A and Fortunato E 2013 Recyclable, flexible, low-power oxide electronics *Adv. Funct. Mater.* **23** 2153-61
- [24] Lim W, Douglas E A, Kim S H, Norton D P, Pearton S J, Ren F, Shen H and Chang W H 2009 High mobility InGaZnO₄ thin-film transistors on paper *Appl. Phys. Lett.* **94** 072103
- [25] Hu L et al 2013 Transparent and conductive paper from nanocellulose fibers *Energy Environ. Sci.* **6** 513
- [26] Nystrom G, Mhryan A, Razaq A, Lindstrom T, Nyholm L and Strømme M 2010 A nanocellulose polypyrrole composite based on microfibrillated cellulose from wood *J. Phys. Chem. B* **114** 4178-82
- [27] Tanaka T, Sano E, Imai M and Akiyama K 2010 Electrical conductivity of carbon-nanotube/cellulose composite paper *J. Appl. Phys.* **107** 054307
- [28] Huang L, Chen K, Peng C and Gerhardt R A 2011 Highly conductive paper fabricated with multiwalled carbon nanotubes and poly(3,4-ethylenedioxythiophene)-poly(styrenesulfonate) by unidirectional drying *J. Mater. Sci.* **4** 6648-55
- [29] Luong N D, Pahimanolis N, Hippi U, Korhonen J T, Ruokolainen J, Johansson L-S, Nam J-D and Seppälä J 2011 Graphene/cellulose nanocomposite paper with high electrical and mechanical performances *J. Mater. Chem.* **21** 13991-8
- [30] Zhang W, Zhang X D, Lu C H, Wang Y J and Deng Y L 2012 Flexible and transparent paper-based ionic diode fabricated from oppositely charged microfibrillated cellulose *J. Phys. Chem. C* **116** 9227-34
- [31] Barquinha P, Pereira L, Goncalves G, Martins R and Fortunato E 2008 The effect of deposition conditions and annealing on the performance of high-mobility GIZO TFTs *Electrochem. Solid State Lett.* **11** H248-51
- [32] Segal J J C L, Martin A E Jr and Conrad C M 1959 An empirical method for estimating the degree of crystallinity of native cellulose using the x-ray diffractometer *Textile Res. J.* **29** 786-94
- [33] Park S, Baker J O, Himmel M E, Parilla P A and Johnson D K 2010 Cellulose crystallinity index: measurement techniques and their impact on interpreting cellulose performance *Biotechnol. Biofuels* **3** 10
- [34] Moon R J, Martini A, Nairn Simonsen J and Youngblood J 2011 Cellulose nanomaterials review: structure, properties and nanocomposites *Chem. Soc. Rev.* **40** 3941-94
- [35] Iwamoto S, Nakagaito A N and Yano H 2007 Nano-fibrillation of pulp fibers for the processing of transparent nanocomposites *Appl. Phys. A* **89** 461-6
- [36] Larsson P T 2012 *Determining the Specific Surface Area of NFC by CP/MAS 13C-NMR Recent Advances in Cellulose Nanotechnology Research* PFI, Trondheim Nov.
- [37] Wassana Y 2001 Kinetic and equilibrium analysis of metal ion adsorption onto bleached and unbleached Kraft pulps *PhD Thesis* Oregon State University 181p
- [38] Schwanninger M, Rodrigues J C, Pereira H and Hinterstoisser B 2004 Effects of short-time vibratory ball milling on the shape of FT-IR spectra of wood and cellulose *Vib. Spectrosc.* **36** 23-40
- [39] Olsson A M and Salmen L 2004 The association of water to cellulose and hemicellulose in paper examined by FTIR spectroscopy *Carbohydr. Res.* **339** 813-8
- [40] Proniewicz L M, Paluszkiwicz C, Weselucha-Birczysimska A, Majcherczyk H, Baranski A and Konieczna A 2001 FT-IR and FT-Raman study of hydrothermally degraded cellulose *J. Mol. Struct.* **596** 163-9
- [41] Oh S Y, Yoo D I, Shin Y and Seo G 2005 FTIR analysis of cellulose treated with sodium hydroxide and carbon dioxide *Carbohydr. Res.* **340** 417-28
- [42] Lojewska J, Miskowicz P, Lojewski T and Proniewicz L M 2005 Cellulose oxidative and hydrolytic degradation: *in situ* FTIR approach *Polym. Degrad. Stab.* **88** 512-20
- [43] Marchessault R H 1962 Application of infra-red spectroscopy to cellulose and wood polysaccharides *Pure Appl. Chem.* **5** 107-29
- [44] Grdadolnik J and Maréchal Y 2001 Bovine serum albumin observed by infrared spectrometry. I. Methodology, structural investigation, and water uptake *Biospectroscopy* **62** 40-53
- [45] Kalichevsky M T, Jaroszkiewicz E M, Ablett S, Blanshard J M V and Lillford P J 1992 The glass transition of amylopectin measured by DSC, DMTA and NMR *Carbohydr. Polym.* **18** 77-88
- [46] Peng Y, Gardner D J and Han Y 2012 Drying cellulose nanofibrils: in search of a suitable method *Cellulose* **19** 91-102
- [47] Beran A 1986 A model of water allocation in alkali feldspar, derived from infrared-spectroscopic investigations *Phys. Chem. Miner.* **13** 306-10
- [48] Larsson O, Said E, Berggren M and Crispin X 2009 Insulator polarization mechanisms in polyelectrolyte-gated organic field-effect transistors *Adv. Funct. Mater.* **19** 3334-41
- [49] Ma L and Yang Y 2005 Solid-state supercapacitors for electronic device applications *Appl. Phys. Lett.* **87** 123503
- [50] Sandberg H G O, Backlund T G, Osterbacka R and Stubb H 2004 High-performance all-polymer transistor utilizing a hygroscopic insulator *Adv. Mater.* **16** 1112
- [51] Panzer M J and Frisbie C D 2008 Exploiting ionic coupling in electronic devices: electrolyte-gated organic field-effect transistors *Adv. Mater.* **20** 3176
- [52] Dasgupta S, Gottschalk S, Kruk R and Hahn H 2008 A nanoparticulate indium tin oxide field-effect transistor with solid electrolyte gating *Nanotechnology* **19** 435203
- [53] Yuan H, Shimotani H, Tsukazaki A, Ohtomo A, Kawasaki M and Iwasa Y 2010 Hydrogenation-induced surface polarity recognition and proton memory behavior at protic-ionic-liquid/oxide electric-double-layer interfaces *J. Am. Chem. Soc.* **132** 6672-8
- [54] Martins R et al 2011 Away from silicon era: the paper electronics *Proc. SPIE* **7940** 79400P
- [55] Fortunato E, Barquinha P and Martins R 2012 Oxide semiconductor thin-film transistors: a review of recent advances *Adv. Mater.* **24** 2945-86
- [56] Martins R, Barquinha P, Pereira L, Correia N, Gonçalves G, Ferreira I and Fortunato E 2009 Selective floating gate non-volatile paper memory transistor *Phys. Status Solidi RRL* **3** 308-10
- [57] Suo Z, Ma E Y, Gleskova H and Wagner S 1999 Mechanics of rollable and foldable film-on-foil electronics *Appl. Phys. Lett.* **74** 1177-9
- [58] Sekitani T, Zschieschang U, Klauk H and Someya T 2010 Flexible organic transistors and circuits with extreme bending stability *Nature Mater.* **9** 1015-22
- [59] Xia Y, Zhang W, Ha M, Cho J H, Renn M J, Kim C H and Frisbie C D 2010 Printed sub-2 V gel-electrolyte-gated polymer transistors and circuits *Adv. Funct. Mater.* **20** 1-8